Heat transfer correlations for vaporizing liquid droplet arrays in a high-temperature gas at intermediate Reynolds number

Albert Y. Tong and Steven J. Chen
Mechanical Engineering Department, The University of Texas at Arlington, Arlington, TX, USA

Received 19 September 1986 and accepted for publication 29 April 1987

The objective of the present study is to investigate the effects of droplet spacing on the heat and mass transfer characteristics of an individual droplet in a liquid fuel spray. The goal is to obtain a mathematical relationship between heat and mass transfer rates and local ambient properties which can be applied directly as an input for a complete liquid spray analysis. A three-droplet array in a cylindrical duct is used. The Navier-Stokes equations in vorticity-stream-function form and the energy equation are solved numerically by using a finite difference method with nonuniform cylindrical mesh. Nusselt number correlations for both the vaporizing and the nonvaporizing droplet array cases have been obtained.

Keywords: heat transfer; drop; numerical modeling

Introduction

The combustion of liquid fuel sprays is of substantial practical importance. It is involved in many combustion systems such as liquid rocket engines, afterburners, carburetors, and ramjets. The temperature inside a combustion chamber is typically high. The liquid fuel droplets injected inside the chamber undergo vaporization and, subsequently, combustion. In many practical situations, vaporization can be the rate-controlling factor. Thus, studies on the vaporization and combustion of the sprays are of vital importance for improving the performance of combustion systems using spray injections. However, the physical phenomena of evaporating and combusting sprays is extremely complicated, and modeling it is very difficult. Alternatively, the behaviors of individual droplets can serve as fundamental inputs for spray analysis.

Most studies on the combustion of liquid fuel sprays consider the vaporization of either single isolated droplets or overall droplet sprays, and relatively few works have been done on interactions between droplets. Extensive reviews have been given by Williams,[1] Faeth,[2] Law,[3] and Sirignano.[4]

In real combustors, the Reynolds number based on fuel droplet diameter can be as high as several hundreds. Hence, the local mass and heat transfer around a droplet is not spherically symmetric. The droplet is initially cold and heats up with time. The transient droplet heat-up effect can be significant. Also, real fuels are not pure but multicompositional, with varying volatilities for the components. Nevertheless, classical droplet vaporization theory treats isolated droplets with a single-component, quasi-steady, and spherically symmetric model. It is on the relaxations of these simplifying features that modern developments of droplet vaporization theories are focusing.

The single-droplet theory ignores the effect of the droplet on the ambient properties, but spray vaporization theory considers the influence of all the droplets on the spray and accounts for the full coupling among the properties of the ambient gas and droplets. In a dense spray situation, many droplets are present, and the average distance between droplets can become as low as a few droplet diameters. It is expected that the geometry and scale of the diffusion field surrounding each individual droplet will be affected by droplet interaction. The Nusselt number and the functional form of the relationship between vaporization rates and local ambient conditions will be influenced by the droplet spacing. However, the existing spray combustion analyses have not included droplet interaction, but have considered only the oversimplified classical vaporization model for isolated single droplets. Although the spray vaporization models attempt to examine the combustion characteristics of the overall spray, it is essential that the droplet behavior be properly represented. Clearly, an understanding of the effects of droplet spacing on the vaporization characteristic of individual droplet is needed. Of course, it would be too complicated and consume too much computer time to incorporate any detailed droplet model in an already involved analysis of spray vaporization in a combustor. Instead, a mathematical relationship between vaporization rates and local ambient properties which can be applied directly as an input for a complete spray model is more desirable.

Therefore the objective of the present study is to investigate the effects of droplet spacing on the vaporization characteristic of an individual droplet in a spray and to seek a more realistic representation of the vaporization law in a complete spray analysis.

Some investigators have examined a few droplets in a well-defined geometry or many droplets in a periodic configuration. These arrangements are referred to as droplet arrays. Although artificial, these arrays can be very useful in obtaining information on the effect of droplet spacing on transport rates. Some work on heat and mass transfer to an array of nonvaporizing droplets with forced convection has been performed by Tal *et al.*[5–8] In these studies, an infinite array of spheres of radius a with a uniform spacing $2b$ (Figure 1) is considered. Due to symmetry and the nearly periodic character associated with an infinite array, no heat transfer or momentum transfer takes place at the streamwise equidistant plane between the spheres. By this assumption, the problem is reduced to a multitude of spheres in tandem in a square stream tube (Figure 2). Because this is clearly a three-dimensional problem and appears to be intractable even with the latest numerical

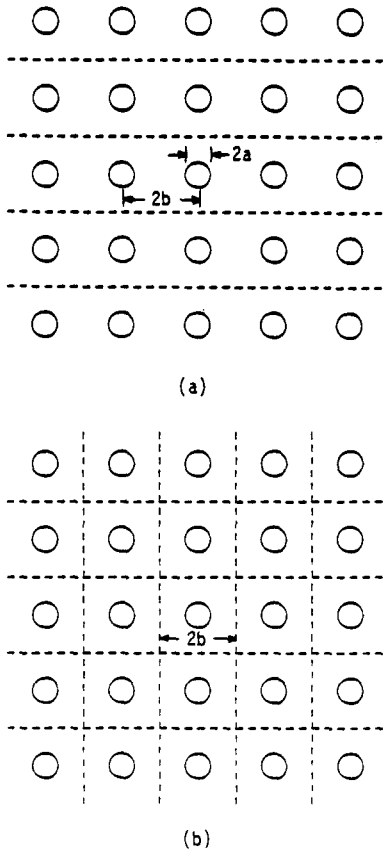

Figure 1 Assemblage geometry: (a) side view; (b) front view

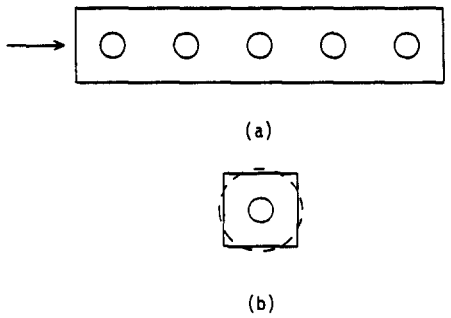

Figure 2 Multisphere cylindrical cell: (a) side view; (b) front view

techniques, the square duct is replaced with a cylindrical duct of equal cross-sectional area.

The Navier-Stokes equations in vorticity-stream-function form and the energy equation are solved numerically by a finite difference method with nonuniform cylindrical mesh. The diffusion terms are expressed by a central difference scheme and the convective terms (in both the vorticity and the energy equation) by an upwind difference scheme. The nonlinear coupling of the stream function equation and the vorticity equation are solved by iteration.

It has been found that strong interaction between the flow fields surrounding neighboring droplets occurs when the droplet centers are less than two droplet diameters apart.

In the present study, an approach similar to Tal's work has been adopted, although the governing equations as well as the numerical formulation are obtained independently. A study on grid spacing has been performed, and an optimum grid has been determined. In order to decrease the amount of false diffusion

Notation

a Radius of droplet, $a=1$
$2b$ Distance between the centers of two neighbor droplets
B Mass transfer number, $B=C_p(T_i'-T_s')/L'$
C_p Specific heat at constant pressure
d Diameter of droplet, $d=2a$
D Mass diffusivity
F Generalized variable representing U, ψ, or T
h Heat transfer coefficient
k Thermal conductivity
L' Heat of vaporization
L Dimensionless heat of vaporization, $L=L'/C_p(T_i'-T_s')$
Nu_θ Local Nusselt number
$\overline{\mathrm{Nu}}$ Average Nusselt number, $\overline{\mathrm{Nu}}=hd/k$
Pr Prandtl number, $\mathrm{Pr}=C_p\mu/k$
r' Radial coordinate in cylindrical coordinate system
Re Reynolds number, $\mathrm{Re}=\rho v_i' d/\mu$
Sc Schmidt number, $\mathrm{Sc}=\nu/D$
T' Temperature
T Dimensionless temperature, $T=(T'-T_s')/(T_i'-T_s')$
T_i' Inlet temperature
T_s' Droplet surface temperature
U Normalized dimensionless vorticity, $U=\omega y$
v_i' Inlet velocity
x Dimensionless axial coordinate, $x=z'/a$
X Value of x at outlet
y Dimensionless radial coordinate, $y=r'/a$
Y Normalized mass fraction of evaporating species, $Y=(Y'-Y_s')/Y_s'$
z' Axial coordinate in cylindrical coordinate system

Greek symbols
α Thermal diffusivity, $\alpha=k/\rho C_p$
θ Angle from frontal stagnation point
μ Dynamic viscosity
ν Kinematic viscosity
ρ Density
ϕ' Azimuthal coordinate in cylindrical coordinate system
ψ' Stream function
ψ Dimensionless stream function, $\psi=\psi'/v_i'a^2$
ω' Vorticity
ω Dimensionless vorticity, $\omega=\omega' a/v_i'$

Superscripts
$'$ Dimensional quantity
$-$ Averaged quantity

Subscripts
s Droplet surface
i Inlet
n Normal to the droplet surface

caused by the upwind difference scheme, the hybrid scheme is used instead. The formulation has also been extended to the vaporizing droplet case. Nusselt number correlations for both vaporizing and nonvaporizing droplet cases have been obtained. These correlations can be useful in a complete spray analysis.

Mathematical formulation

The vorticity equation for an axisymmetric flow in cylindrical coordinates is given by

$$v'_{r'}\frac{\partial\omega'}{\partial r'}+v'_{z'}\frac{\partial\omega'}{\partial z'}-\frac{v'_{r'}}{r'}\omega'=\nu\left[\frac{\partial^2\omega'}{\partial r'^2}+\frac{\partial^2\omega'}{\partial z'^2}+\frac{1}{r'}\frac{\partial\omega'}{\partial r'}-\frac{\omega'}{r'^2}\right] \tag{1}$$

where ω' is the component of the vorticity given by

$$\omega'=\frac{\partial v'_{z'}}{\partial r'}-\frac{\partial v'_{r'}}{\partial z'} \tag{2}$$

The vorticity components in the r' and z' axes are everywhere zero for axisymmetric flow. Here, the prime denotes dimensional quantities.

The energy equation expressed in terms of temperature is

$$v'_{r'}\frac{\partial T'}{\partial r'}+v'_{z'}\frac{\partial T'}{\partial z'}=\alpha\left[\frac{1}{r'}\frac{\partial}{\partial r'}\left(r'\frac{\partial T'}{\partial r'}\right)+\frac{\partial^2 T'}{\partial z'^2}\right] \tag{3}$$

Defining a stream function ψ' as

$$v'_r=-\frac{1}{r'}\frac{\partial\psi'}{\partial z'} \tag{4a}$$

$$v'_z=\frac{1}{r'}\frac{\partial\psi'}{\partial r'} \tag{4b}$$

transforms Equations 1–3 to

$$-\frac{1}{r'}\frac{\partial\psi'}{\partial z'}\frac{\partial\omega'}{\partial r'}+\frac{1}{r'}\frac{\partial\psi'}{\partial r'}\frac{\partial\omega'}{\partial z'}+\frac{1}{r'^2}\frac{\partial\psi'}{\partial z'}\omega'=\nu\left[\frac{\partial^2\omega'}{\partial r'^2}+\frac{\partial^2\omega'}{\partial z'^2}+\frac{1}{r'}\frac{\partial\omega'}{\partial r'}-\frac{\omega'}{r'^2}\right] \tag{5}$$

$$\omega'=\frac{1}{r'}\frac{\partial^2\psi'}{\partial r'^2}-\frac{1}{r'^2}\frac{\partial\psi'}{\partial r'}+\frac{1}{r'}\frac{\partial^2\psi'}{\partial z'^2} \tag{6}$$

and

$$-\frac{1}{r'}\frac{\partial\psi'}{\partial z'}\frac{\partial T'}{\partial r'}+\frac{1}{r'}\frac{\partial\psi'}{\partial r'}\frac{\partial T'}{\partial z'}=\alpha\left[\frac{\partial^2 T'}{\partial z'^2}+\frac{\partial^2 T'}{\partial r'^2}+\frac{1}{r'}\frac{\partial T'}{\partial r'}\right] \tag{7}$$

respectively.

If we set

$$\omega=\frac{\omega' a}{v'_i} \tag{8a}$$

$$\psi=\frac{\psi'}{v'_i a^2} \tag{8b}$$

$$T=\frac{T'-T'_s}{T'_i-T'_s} \tag{8c}$$

$$x=\frac{z'}{a} \tag{8d}$$

$$y=\frac{r'}{a} \tag{8e}$$

$$U=\omega y \tag{8f}$$

the governing equations, Equations 5–7, can be nondimensionalized to become

$$\frac{\mathrm{Re}}{2y}\left[\frac{\partial\psi}{\partial y}\frac{\partial U}{\partial x}-\frac{\partial\psi}{\partial x}\frac{\partial U}{\partial y}\right]+\frac{\mathrm{Re}\,U}{y^2}\frac{\partial\psi}{\partial x}=\frac{\partial^2 U}{\partial x^2}+\frac{\partial^2 U}{\partial y^2}-\frac{1}{y}\frac{\partial U}{\partial y} \tag{9}$$

$$U=\frac{\partial^2\psi}{\partial x^2}+\frac{\partial^2\psi}{\partial y^2}-\frac{1}{y}\frac{\partial\psi}{\partial y} \tag{10}$$

and

$$\frac{\mathrm{Re}\,\mathrm{Pr}}{2y}\left[\frac{\partial\psi}{\partial y}\frac{\partial T}{\partial x}-\frac{\partial\psi}{\partial x}\frac{\partial T}{\partial y}\right]=\frac{\partial^2 T}{\partial x^2}+\frac{\partial^2 T}{\partial y^2}+\frac{1}{y}\frac{\partial T}{\partial y} \tag{11}$$

The boundary conditions are as follows:

(i) at the inlet ($x=0$):

$$\psi=\tfrac{1}{2}y^2 \tag{12}$$

$$U=0 \tag{13}$$

$$T=1 \tag{14}$$

(ii) at the axis of symmetry ($y=0$):

$$\psi=0 \tag{15}$$

$$U=0 \tag{16}$$

$$\frac{\partial T}{\partial y}=0 \tag{17}$$

(iii) at the outlet ($x=X$):

$$\frac{\partial\psi}{\partial x}=0 \tag{18}$$

$$\frac{\partial U}{\partial x}=0 \tag{19}$$

$$\frac{\partial T}{\partial x}=0 \tag{20}$$

(iv) at the cylinder wall $\left(y=\frac{b}{a}\left(\frac{4}{\pi}\right)^{1/2}\right)$:

$$\psi=\frac{2}{\pi}\left(\frac{b}{a}\right)^2 \tag{21}$$

$$U=0 \tag{22}$$

$$\frac{\partial T}{\partial y}=0 \tag{23}$$

(v) at the droplet surface:

$$\psi=0 \tag{24}$$

$$\frac{\partial\psi}{\partial n}=0 \tag{25}$$

$$T=0 \tag{26}$$

The above formulation is valid for the nonvaporizing droplet case. Prakash[9] found that the surface velocity is typically small and does not greatly affect the heat and mass transfers or the vaporization rate in the gas phase. Hence, the surface velocity can be neglected in the gas-phase analysis. This greatly simplifies the problem, because the matching of the surface velocity along the droplet surface is eliminated. Although this approximation leads to the physically unrealistic slip condition at the interface, it is believed that the solution will not be affected significantly.

The formulation has been extended to the vaporizing droplet case. Here the gas-phase quasi-steadiness assumption is again utilized, which justifies the freezing of the droplet properties and parameters for the gas-phase calculation. The governing

equations previously derived remain valid, but a species equation is needed. This equation, similar to the energy equation, is

$$\frac{\mathrm{Re\,Sc}}{2y}\left[\frac{\partial\psi}{\partial y}\frac{\partial Y}{\partial x}-\frac{\partial\psi}{\partial x}\frac{\partial Y}{\partial y}\right]=\frac{\partial^2 Y}{\partial x^2}+\frac{\partial^2 Y}{\partial y^2}+\frac{1}{y}\frac{\partial Y}{\partial y}$$

The current vaporization model does not account for droplet heating. It assumes that the droplet temperature remains uniform at the wet-bulb temperature, which corresponds to the free-stream temperature. The concentration of the evaporating species at the droplet surface is determined from its equilibrium vapor pressure, which is obtained from the Clausius-Clapeyron equation. The boundary conditions previously stated remain unchanged except for Equation 24, which becomes

$$\frac{\partial\psi}{\partial\theta}=-\frac{2\sin\theta}{L\,\mathrm{Re\,Pr}}\frac{\partial T}{\partial n}$$

This equation accounts for the vaporization mass flux at the droplet surface. The symbol L is the nondimensionalized latent heat of vaporization.

The local heat transfer to the droplet can be expressed in terms of the local Nusselt number

$$\mathrm{Nu}_\theta=2\frac{\partial T}{\partial n} \tag{27}$$

Subsequently, the overall average heat transfer to the whole droplet can be expressed as

$$\overline{\mathrm{Nu}}=\frac{1}{2}\int_0^\pi \mathrm{Nu}_\theta\sin\theta\,\mathrm{d}\theta \tag{28}$$

Finite difference formulation

By using finite difference approximations, we can reduce the governing equations to a set of nonlinear algebraic equations that can be solved by an iteration scheme. We use a line-by-line successive underrelaxation method with a hybrid scheme. As pointed out in Ref. 10, the hybrid scheme has some advantages over the upwind and central difference schemes. The finite difference forms of the governing equations with nonuniform spacing are derived below.

For nonuniform spacing (Figure 3) the partial derivatives of a function F at grid location 0 expressed in a central difference form are given by the following expressions:

$$\left.\frac{\partial F}{\partial x}\right|_0=\frac{(A^2-B^2)F_0+B^2F_1-A^2F_3}{AB(A+B)} \tag{29}$$

$$\left.\frac{\partial F}{\partial y}\right|_0=\frac{(C^2-D^2)F_0+D^2F_2-C^2F_4}{CD(C+D)} \tag{30}$$

$$\left.\frac{\partial^2 F}{\partial x^2}\right|_0=\frac{2BF_1+2AF_3-2(A+B)F_0}{AB(A+B)} \tag{31}$$

$$\left.\frac{\partial^2 F}{\partial y^2}\right|_0=\frac{2DF_2+2CF_4-2(C+D)F_0}{CD(C+D)} \tag{32}$$

Here F is a generalized function representing T, ψ, or U. Substituting these expressions into Equation 11 yields the following terms:

(i) First term on the left side:

$$\frac{\mathrm{Re\,Pr}}{2y}\frac{\partial\psi}{\partial y}\frac{\partial T}{\partial x}=C_{10}T_0-C_{11}T_1-C_{13}T_3$$

where

$$C_{11}=-\frac{\mathrm{Re\,Pr}}{2y}\frac{\partial\psi}{\partial y}\frac{B^2}{AB(A+B)}$$

$$C_{13}=\frac{\mathrm{Re\,Pr}}{2y}\frac{\partial\psi}{\partial y}\frac{A^2}{AB(A+B)} \tag{33}$$

$$C_{10}=C_{11}+C_{13}$$

(ii) Second term on the left side:

$$\frac{\mathrm{Re\,Pr}}{2y}\left(-\frac{\partial\psi}{\partial x}\right)\frac{\partial T}{\partial y}=C_{20}T_0-C_{22}T_2-C_{24}T_4$$

where

$$C_{22}=-\frac{\mathrm{Re\,Pr}}{2y}\left(-\frac{\partial\psi}{\partial x}\right)\frac{D^2}{CD(C+D)}$$

$$C_{24}=\frac{\mathrm{Re\,Pr}}{2y}\left(-\frac{\partial\psi}{\partial x}\right)\frac{C^2}{CD(C+D)} \tag{34}$$

$$C_{20}=C_{22}+C_{24}$$

(iii) First term on the right side:

$$\frac{\partial^2 T}{\partial x^2}=-C_{40}T_0+C_{41}T_1+C_{43}T_3$$

where

$$C_{41}=\frac{2B}{AB(A+B)}$$

$$C_{43}=\frac{2A}{AB(A+B)} \tag{35}$$

$$C_{40}=C_{41}+C_{43}$$

(iv) Second term on the right side:

$$\frac{\partial^2 T}{\partial y^2}=-C_{50}T_0+C_{52}T_2+C_{54}T_4$$

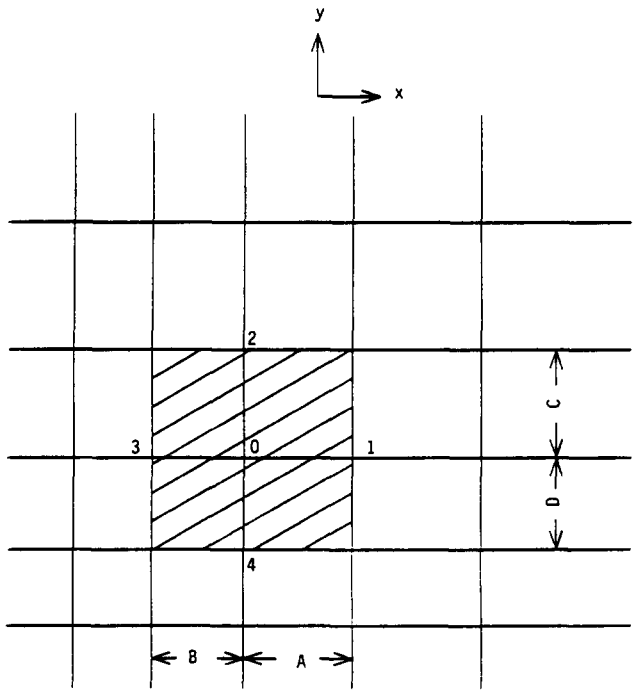

Figure 3 The finite difference grid

where

$$C_{52}=\frac{2D}{CD(C+D)}$$

$$C_{54}=\frac{2C}{CD(C+D)} \tag{36}$$

$$C_{50}=C_{52}+C_{54}$$

(v) The third term on the right side:

$$\frac{1}{y}\frac{\partial T}{\partial y}=-C_{60}T_0+C_{62}T_2+C_{64}T_4$$

where

$$C_{62}=\frac{1}{y}\frac{D^2}{CD(C+D)}$$

$$C_{64}=-\frac{1}{y}\frac{C^2}{CD(C+D)} \tag{37}$$

$$C_{60}=C_{62}+C_{64}$$

After rearranging terms, we obtain the discretization equation

$$C_0T_0=C_1T_1+C_2T_2+C_3T_3+C_4T_4 \tag{38}$$

where

$$\begin{aligned}C_1&=C_{11}+C_{41}\\C_2&=C_{22}+C_{52}+C_{62}\\C_3&=C_{13}+C_{43}\\C_4&=C_{24}+C_{54}+C_{64}\\C_0&=C_1+C_2+C_3+C_4\end{aligned} \tag{39}$$

This discretization formulation is obtained by the central differencing method. For the upwind difference scheme, we use upstream differencing instead of central differencing in the convective terms. The C's given in Equations 33 and 34 become

$$C_{11}=\frac{\mathrm{Re}\,\mathrm{Pr}}{2y}\frac{A_2}{A}$$

$$C_{13}=\frac{\mathrm{Re}\,\mathrm{Pr}}{2y}\frac{A_1}{B} \tag{40}$$

$$C_{10}=C_{11}+C_{13}$$

and

$$C_{22}=\frac{\mathrm{Re}\,\mathrm{Pr}}{2y}\frac{B_2}{C}$$

$$C_{24}=\frac{\mathrm{Re}\,\mathrm{Pr}}{2y}\frac{B_1}{D} \tag{41}$$

$$C_{20}=C_{22}+C_{24}$$

where

$$\begin{aligned}A_1&=\left[\left|\frac{\partial\psi}{\partial y},0\right|\right]\\A_2&=\left[\left|-\frac{\partial\psi}{\partial y},0\right|\right]\\B_1&=\left[\left|-\frac{\partial\psi}{\partial x},0\right|\right]\\B_2&=\left[\left|\frac{\partial\psi}{\partial x},0\right|\right]\end{aligned} \tag{42}$$

The symbol [| |] stands for the largest quantity contained within it. It is equivalent to AMAX1 in the FORTRAN language. The discretization equations, Equations 38 and 39, remain the same.

In the present study, the hybrid scheme is used. It is basically a combination of the central difference and upwind difference schemes. The central difference scheme is utilized when the following conditions are satisfied:

$$\frac{\mathrm{Re}\,\mathrm{Pr}}{2y}\frac{\partial\psi}{\partial y}B<2 \quad\text{and}\quad \frac{\mathrm{Re}\,\mathrm{Pr}}{2y}\frac{\partial\psi}{\partial y}A>-2$$

for x direction and

$$\left[\frac{\mathrm{Re}\,\mathrm{Pr}}{2y}\left(-\frac{\partial\psi}{\partial x}\right)-\frac{1}{y}\right]D<2 \quad\text{and}\quad \left[\frac{\mathrm{Re}\,\mathrm{Pr}}{2y}\left(-\frac{\partial\psi}{\partial x}\right)-\frac{1}{y}\right]C>-2$$

for y direction.

Otherwise, the upwind difference scheme will be used. In that situation regime, the Peclet number is large and the flow is convection dominating, which results in a flat profile with negligible diffusion at the cell boundary. The upwind difference scheme always calculates the diffusion term from a linear profile and thus overestimates diffusion at large Peclet numbers. In the hybrid scheme, the diffusion term is set to zero (i.e., C_{41}, C_{43}, C_{40}, C_{52}, and C_{54} are zero). Thus the shortcoming of the upwind scheme is eliminated.

The same procedure can be applied to obtain discretization equations for the vorticity and stream function equations, Equations 9 and 10. For the vorticity equation, we have

$$\frac{\mathrm{Re}}{2y}\left[\frac{\partial\psi}{\partial y}\frac{\partial U}{\partial x}-\frac{\partial\psi}{\partial x}\frac{\partial U}{\partial y}\right]+\frac{\mathrm{Re}\,U}{y^2}\frac{\partial\psi}{\partial x}=\frac{\partial^2U}{\partial x^2}+\frac{\partial^2U}{\partial y^2}-\frac{1}{y}\frac{\partial U}{\partial y}$$

Replacing the derivatives by finite difference formulations gives the following expressions:

(i) First term on the left side:

$$\frac{\mathrm{Re}}{2y}\frac{\partial\psi}{\partial y}\frac{\partial U}{\partial x}=D_{10}U_0-D_{11}U_1-D_{13}U_3$$

where

$$D_{11}=-\frac{\mathrm{Re}}{2y}\frac{\partial\psi}{\partial y}\frac{B^2}{AB(A+B)}$$

$$D_{13}=\frac{\mathrm{Re}}{2y}\frac{\partial\psi}{\partial y}\frac{A^2}{AB(A+B)} \tag{43}$$

$$D_{10}=D_{11}+D_{13}$$

(ii) Second term on the left side:

$$\frac{\mathrm{Re}}{2y}\left(-\frac{\partial\psi}{\partial x}\right)\frac{\partial U}{\partial y}=D_{20}U_0-D_{22}U_2-D_{24}U_4$$

where

$$D_{22}=-\frac{\mathrm{Re}}{2y}\left(-\frac{\partial\psi}{\partial x}\right)\frac{D^2}{CD(C+D)}$$

$$D_{24}=\frac{\mathrm{Re}}{2y}\left(-\frac{\partial\psi}{\partial x}\right)\frac{C^2}{CD(C+D)} \tag{44}$$

$$D_{20}=D_{22}+D_{24}$$

(iii) Third term on the left side:

$$\frac{\mathrm{Re}}{y^2}U\frac{\partial\psi}{\partial x}=D_{30}U_0$$

where

$$D_{30}=\frac{\mathrm{Re}}{y^2}\frac{\partial\psi}{\partial x} \tag{45}$$

(iv) The terms on the right side:

$$\frac{\partial^2 U}{\partial x^2} = -C_{40}U_0 + C_{41}U_1 + C_{43}U_3$$

$$\frac{\partial^2 U}{\partial y^2} = -C_{50}U_0 + C_{52}U_2 + C_{54}U_4$$

$$-\frac{1}{y}\frac{\partial U}{\partial y} = C_{60}U_0 - C_{62}U_2 - C_{64}U_4$$

where the C's are as before.

The discretization equation for the vorticity equation becomes

$$D_0U_0 = D_1U_1 + D_2U_2 + D_3U_3 + D_4U_4 \tag{46}$$

where

$$\begin{aligned} D_1 &= D_{11} + C_{41} \\ D_2 &= D_{22} + C_{52} - C_{62} \\ D_3 &= D_{13} + C_{43} \\ D_4 &= D_{24} + C_{54} - C_{64} \\ D_0 &= D_1 + D_2 + D_3 + D_4 + D_{30} \end{aligned} \tag{47}$$

For the upwind difference scheme, the D's given by Equations 43 and 44 become

$$\begin{aligned} D_{11} &= \frac{\mathrm{Re}}{2y}\frac{A_2}{A} \\ D_{13} &= \frac{\mathrm{Re}}{2y}\frac{A_1}{B} \\ D_{10} &= D_{11} + D_{13} \end{aligned} \tag{48}$$

and

$$\begin{aligned} D_{22} &= \frac{\mathrm{Re}}{2y}\frac{B_2}{C} \\ D_{24} &= \frac{\mathrm{Re}}{2y}\frac{B_1}{D} \\ D_{20} &= D_{22} + D_{24} \end{aligned} \tag{49}$$

For the hybrid scheme, central difference is used when

$$\frac{\mathrm{Re}}{2y}\frac{\partial \psi}{\partial y}B < 2 \quad \text{and} \quad \frac{\mathrm{Re}}{2y}\frac{\partial \psi}{\partial y}A > -2$$

for the x direction and

$$\left[\frac{\mathrm{Re}}{2y}\left(-\frac{\partial \psi}{\partial x}\right) + \frac{1}{y}\right]D < 2 \quad \text{and} \quad \left[\frac{\mathrm{Re}}{2y}\left(-\frac{\partial \psi}{\partial x}\right) + \frac{1}{y}\right]C > -2$$

for the y direction. Outside these ranges, upwind difference is used with the diffusion term set equal to zero, as explained earlier.

Finally, for the stream function equation, Equation 10, we have

$$\frac{\partial^2 \psi}{\partial x^2} = -C_{40}\psi_0 + C_{41}\psi_1 + C_{43}\psi_3$$

$$\frac{\partial^2 \psi}{\partial y^2} = -C_{50}\psi_0 + C_{52}\psi_2 + C_{54}\psi_4$$

$$-\frac{1}{y}\frac{\partial \psi}{\partial y} = C_{60}\psi_0 - C_{62}\psi_2 - C_{64}\psi_4$$

and Equation 10 becomes

$$E_0\psi_0 = E_1\psi_1 + E_2\psi_2 + E_3\psi_3 + E_4\psi_4 - U_0 \tag{50}$$

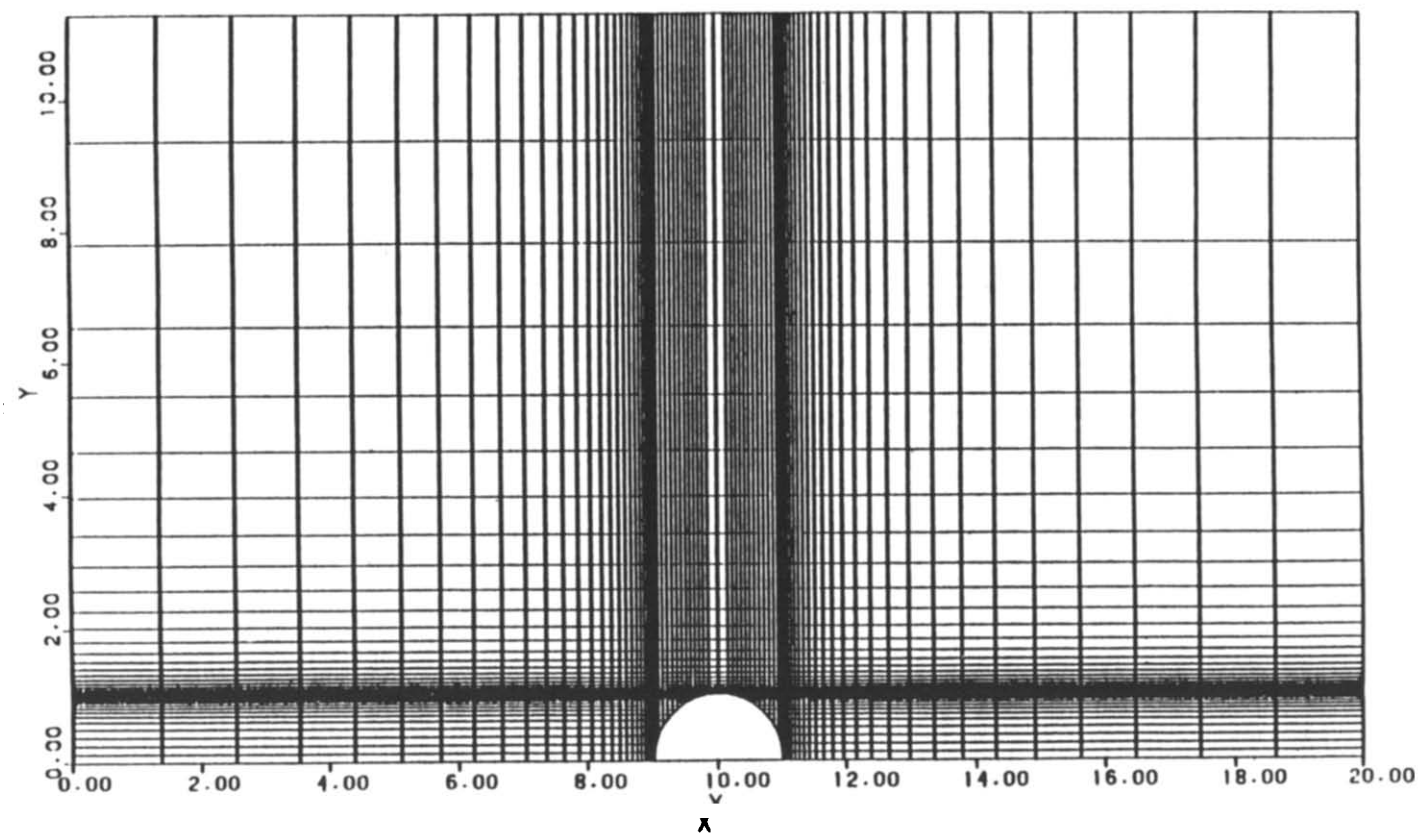

Figure 4 Nonuniform mesh geometry for single droplet

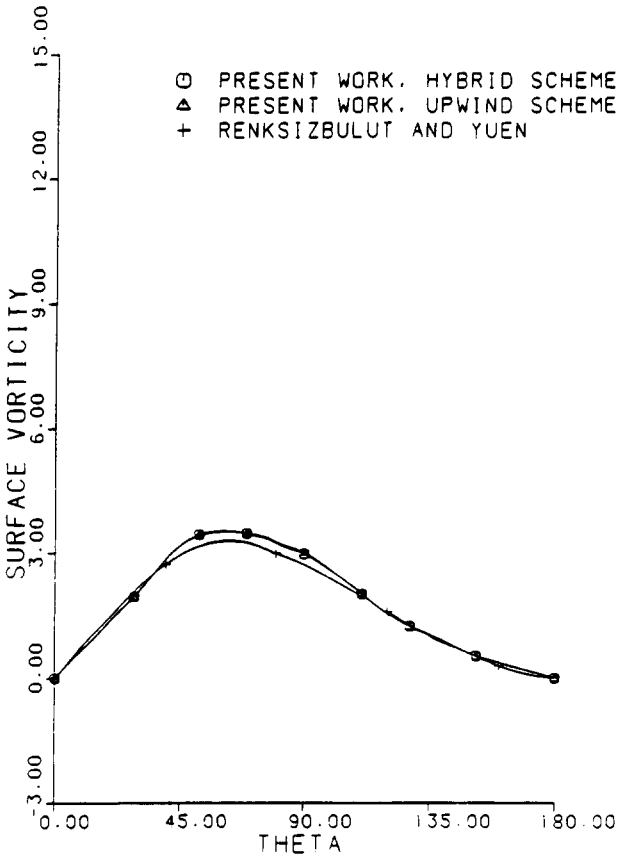

Figure 5 Surface vorticity comparison for Re=10

where

$$E_1 = C_{41}$$
$$E_2 = C_{52} - C_{62}$$
$$E_3 = C_{43} \tag{51}$$
$$E_4 = C_{54} - C_{64}$$
$$E_0 = E_1 + E_2 + E_3 + E_4$$

Equations 38, 46, and 50 form a set of nonlinear algebraic equations which can be solved by an iteration scheme. We use a line-by-line successive underrelaxation method.

Results and discussion

In order to examine the accuracy of the hybrid scheme as well as the validity of the cylindrical cell model, results for the nonvaporizing single-droplet case have been obtained. Both the hybrid and upwind schemes are used, and the results are compared with those obtained in Refs. 11 and 12. The mesh geometry for a single droplet is shown in Figure 4. The free-stream boundary conditions are applied at the inlet, outlet, and cell envelope. Numerical solutions have been obtained for Re=10, 50, and 100. Surface vorticity comparisons for Re=10 and 100 are shown in Figures 5 and 6. For a low Reynolds number (Re=10), the results obtained by different schemes are in close agreement. For higher Reynolds numbers (Re=100), the results obtained by using the hybrid scheme are still in good agreement with those of Refs. 11 and 12, but the upwind scheme yields lower values. Similar results have been found in the Nusselt number calculations, which are summarized in Table 1, along with the results from the existing literature. The value of the average Nusselt number calculated by using the hybrid scheme for Re=100 and Pr=0.7 is 6.811, as compared to 5.979 obtained from the upwind scheme, and is closer to the value 6.956 obtained by Renksizbulut and Yuen.[11] The results show that the hybrid scheme yields better agreement with the existing literature than does the upwind scheme.

Numerical solutions have also been obtained for a three-droplet array. The nonuniform mesh geometry with spacing ratio $b/a=1.5$, including an entrance region, is shown in Figure 7. The average Nusselt numbers for Reynolds numbers from 10 to 200, b/a ranging from 1.5 to 4.0, have been obtained. The streamline and isotherm patterns for Re=10, 50, 100, and 150, Pr=1, and $b/a=1.5$ are presented in Figures 8 and 9. The results obtained from Tal *et al.*[6] have been compared with the present results. They are shown in Figures 10 to 12 and in Table 2. The Nusselt numbers obtained in the present study from the upwind scheme are in reasonably close agreement with the values obtained by Tal *et al.*[6] They are lower than the values predicted by the more accurate hybrid scheme.

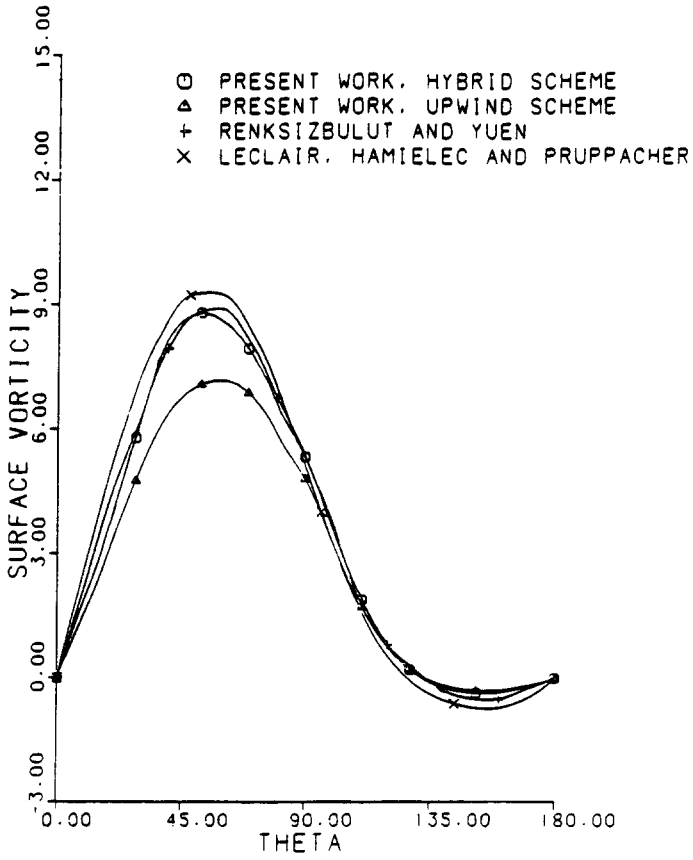

Figure 6 Surface vorticity comparison for Re=100

Table 1 Comparison of average Nusselt numbers for nonvaporizing single droplet

Present work		Renksizbulut and Yuen [11]	Remarks
Hybrid scheme	Upwind scheme		
3.478	3.454	3.396	Re=10 Pr=.7
6.811	5.979	6.956	Re=100 Pr=.7

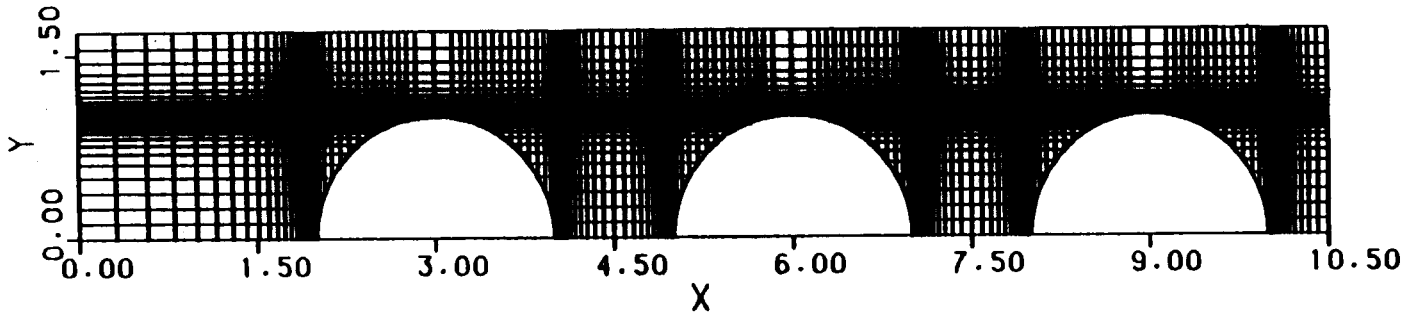

Figure 7 Nonuniform mesh geometry for three-droplet array

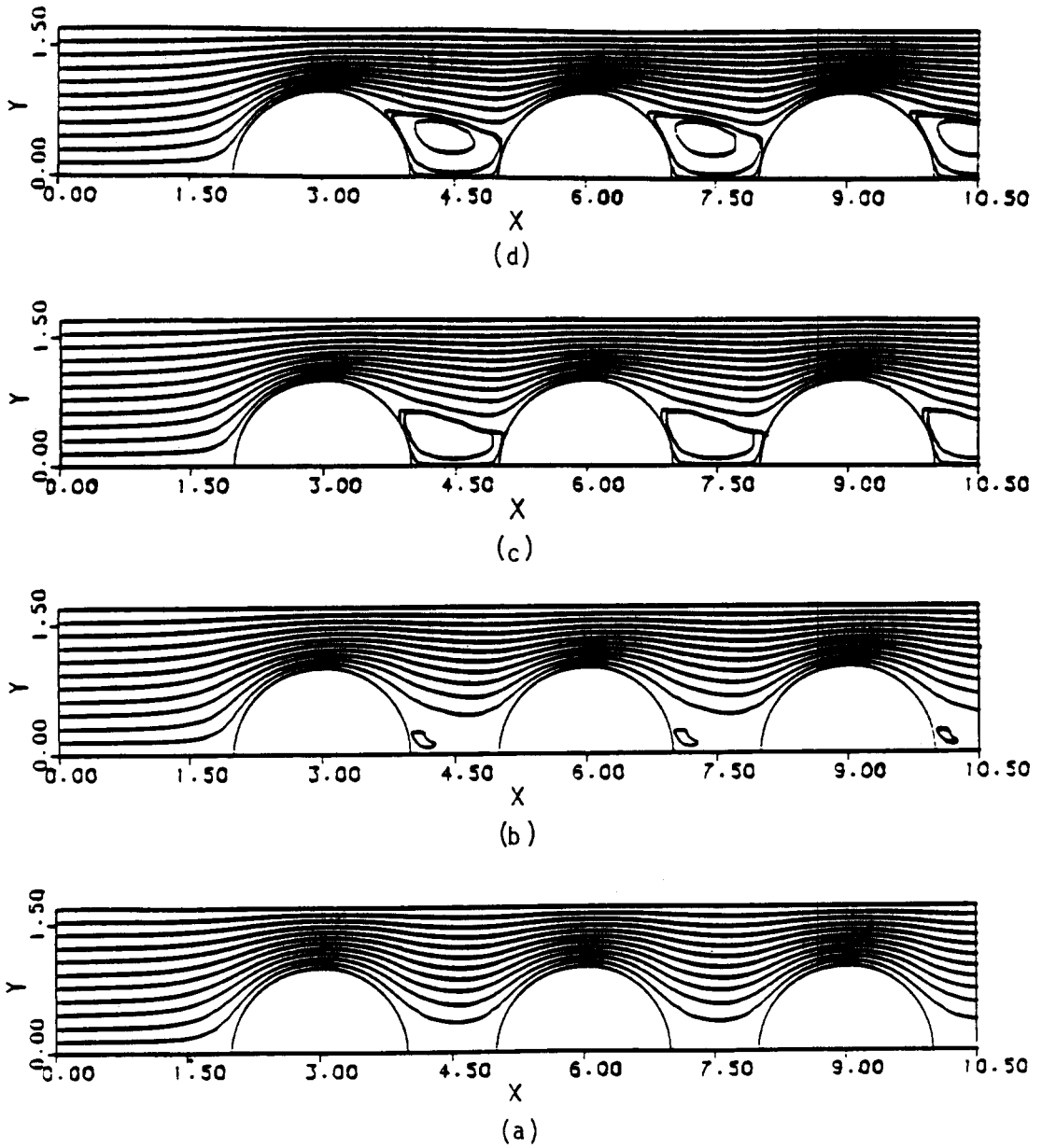

Figure 8 Streamline patterns for three-droplet array, b/a=1.5, Pr=1: (a) Re=10; (b) Re=50; (c) Re=100; (d) Re=150

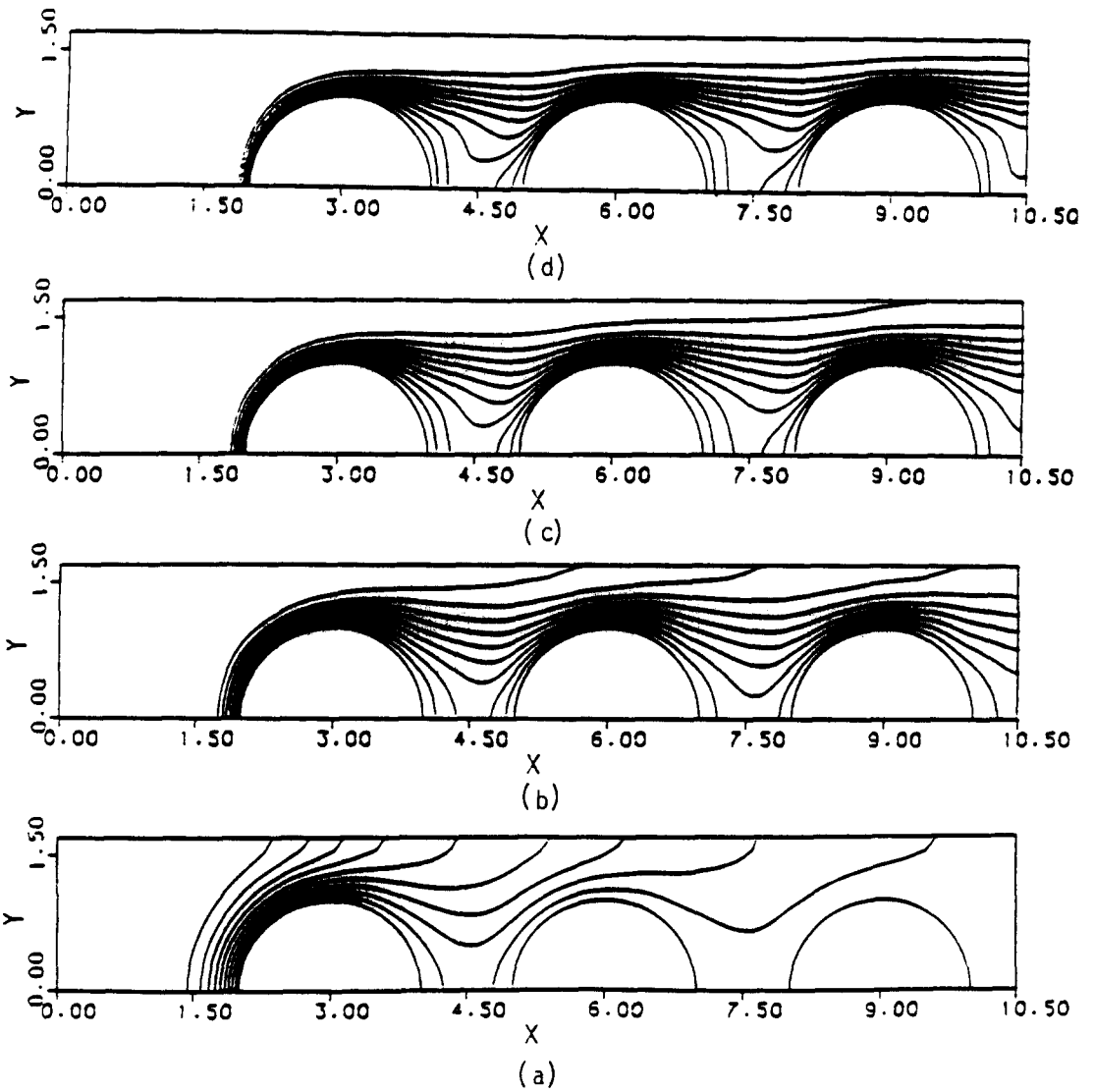

Figure 9 Isotherm patterns for three-droplet array, $b/a=1.5$, Pr=1: (a) Re=10; (b) Re=50; (c) Re=100; (d) Re=150

The effects of entrance length and outlet boundary conditions have been examined. Entrance length has negligible effect on the Nusselt number. An attempt has been made to assume periodic distribution of the flow field and to express the outlet boundary conditions as

$$\psi(X, y)=\psi\left(X-\frac{2b}{a}, y\right)$$

$$U(X, y)=U\left(X-\frac{2b}{a}, y\right)$$

$$\frac{T(X, y)}{T(X-2b/a, y)}=\frac{T(X-2b/a, y)}{T(X-4b/a, y)}$$

No significant change in Nusselt number was detected.

As mentioned earlier, our objective is to investigate the effects of droplet spacing on the vaporization characteristic of an individual droplet in a spray and to obtain a Nusselt number correlation useful in a complete spray analysis. We have tried to correlate the numerical results obtained in the present study, and we have correlated the Nusselt number as a function of the Reynolds number (Re) and droplet spacing (b/a) for each droplet in the three-droplet array.

For the first droplet,

$$\overline{\mathrm{Nu}}=2.219(\mathrm{Re})^{0.306}\left(\frac{b}{a}\right)^{-0.177}$$

For the second droplet,

$$\overline{\mathrm{Nu}}=2.268(\mathrm{Re})^{0.236}\left(\frac{b}{a}\right)^{-0.157}$$

For the third droplet,

$$\overline{\mathrm{Nu}}=2.310(\mathrm{Re})^{0.217}\left(\frac{b}{a}\right)^{-0.172}$$

These correlations correlate the data with a 5% error. The numerical data along with the correlation curves are presented in Figures 13–15.

For evaporating droplets, the vapor leaving the surface interacts with the boundary layer flow, and the thickness of the thermal boundary layer increases. Therefore, the vaporization process lowers the heat transfer to the droplet. Mass transfer numbers from 0 to 3 have been investigated. The effect of vaporization is illustrated in Figures 16 to 18 with plots of the Nusselt number as a function of the Reynolds number. These

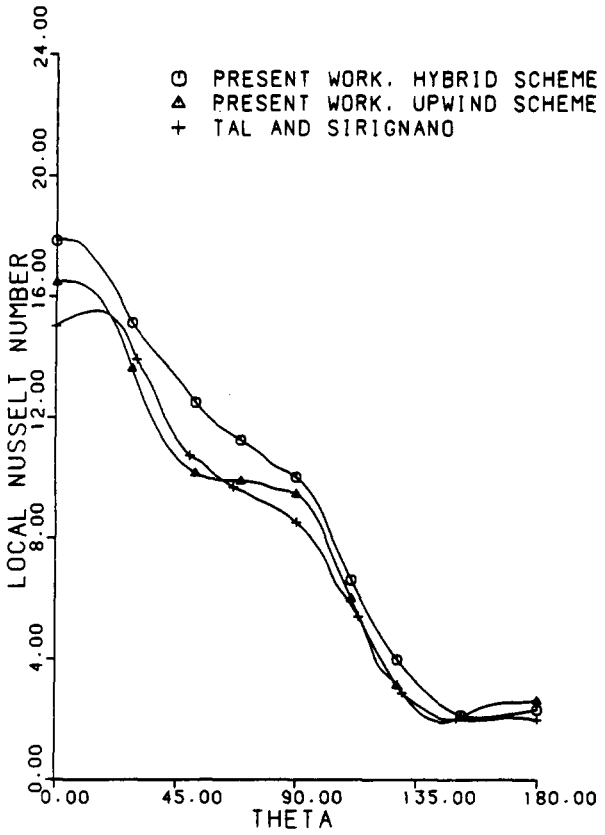

Figure 10 Local Nusselt number comparison for the first droplet of three-droplet array, $b/a=1.5$, Pr=1

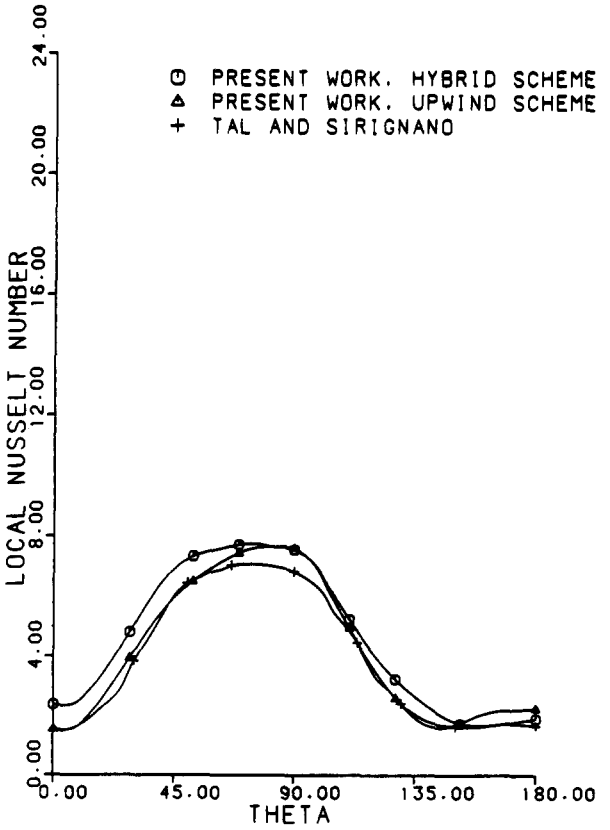

Figure 11 Local Nusselt number comparison for the second droplet of three-droplet array, $b/a=1.5$, Pr=1

plots give the Nusselt number for six values of the mass transfer number, with b/a held constant. At a given mass transfer number, the Nusselt number increases monotonically with the Reynolds number, and the increase is logarithmically linear. The Nusselt numbers for the above-mentioned range of parameters have been correlated by the following equations:

For the first droplet,

$$\overline{\mathrm{Nu}} = 2.272(\mathrm{Re})^{0.309}\left(\frac{b}{a}\right)^{-0.178}(1+B)^{-0.585}$$

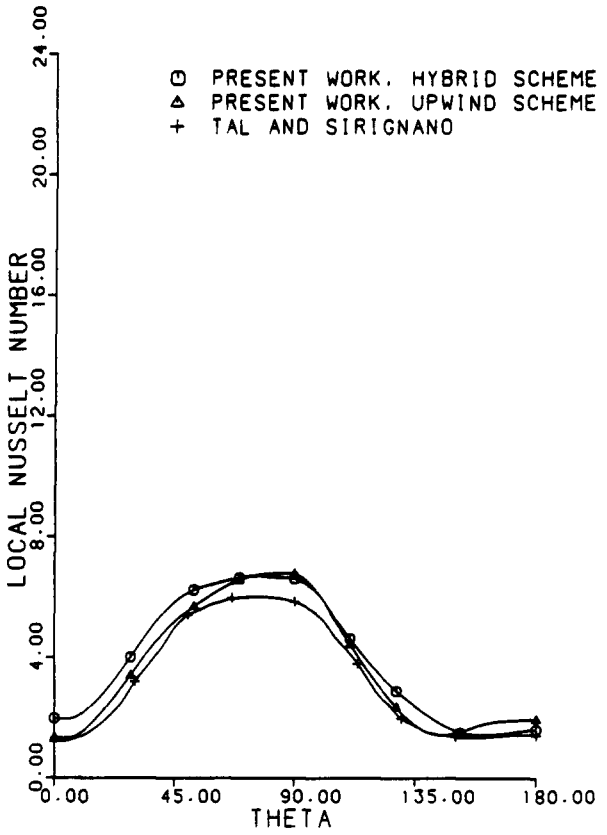

Figure 12 Local Nusselt number comparison for the third droplet of three-droplet array, $b/a=1.5$, Pr=1

Table 2 Comparison of average Nusselt numbers for nonvaporizing three-droplet array: $b/a=1.5$, Re=100, Pr=1

Type of solution	$\overline{\mathrm{Nu}}$ for three-droplet array			Remarks
	First	Second	Third	
Present work hybrid scheme	8.928	5.553	4.809	Based on inlet temperature to the first droplet
Present work upwind scheme	7.869	5.170	4.570	
Tal *et al.*[6] upwind scheme	7.644	4.765	4.061	
Present work hybrid scheme	8.928	6.361	6.030	Based on inlet temperature to each cell unit
Present work upwind scheme	7.869	6.070	5.924	
Tal *et al.*[6] upwind scheme	7.644	6.151	6.270	

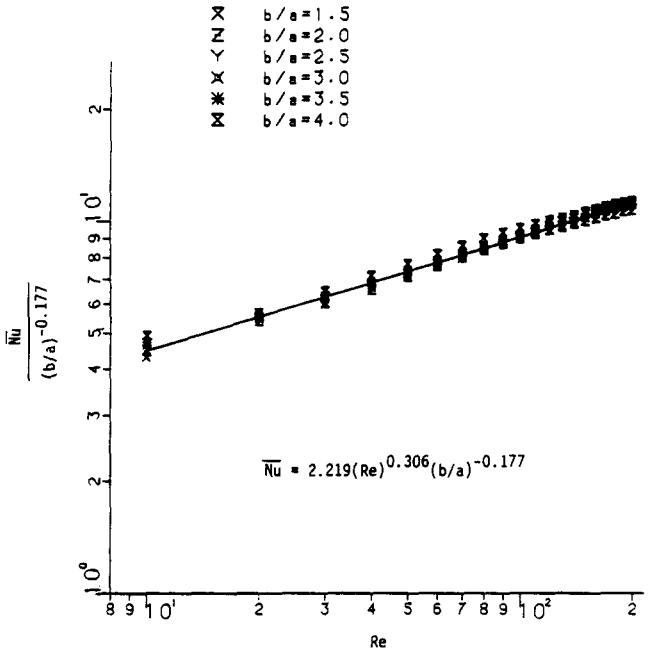

Figure 13 Correlation of Nusselt number for the first droplet of nonvaporizing three-droplet array

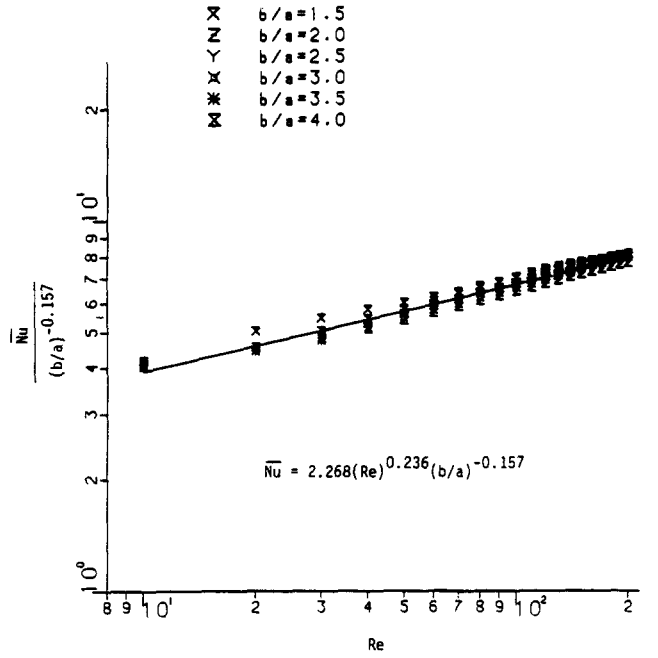

Figure 14 Correlation of Nusselt number for the second droplet of nonvaporizing three-droplet array

For the second droplet,

$$\overline{Nu} = 2.474(Re)^{0.222}\left(\frac{b}{a}\right)^{-0.168}(1+B)^{-0.616}$$

For the third droplet,

$$\overline{Nu} = 2.477(Re)^{0.206}\left(\frac{b}{a}\right)^{-0.191}(1+B)^{-0.601}$$

These correlations and some of the numerical data are presented in Figures 19 to 21. These correlations are by no means universal. They are derived for the parameter ranges considered to be relevant to spray combustion.

The results of this work indicate that the Nusselt number based on the local inlet temperature becomes approximately constant after the first droplet. The second droplet appears to be representative of droplets of the droplet array. As mentioned earlier, our goal is to obtain a mathematical relationship between transfer rate and local ambient properties which can be

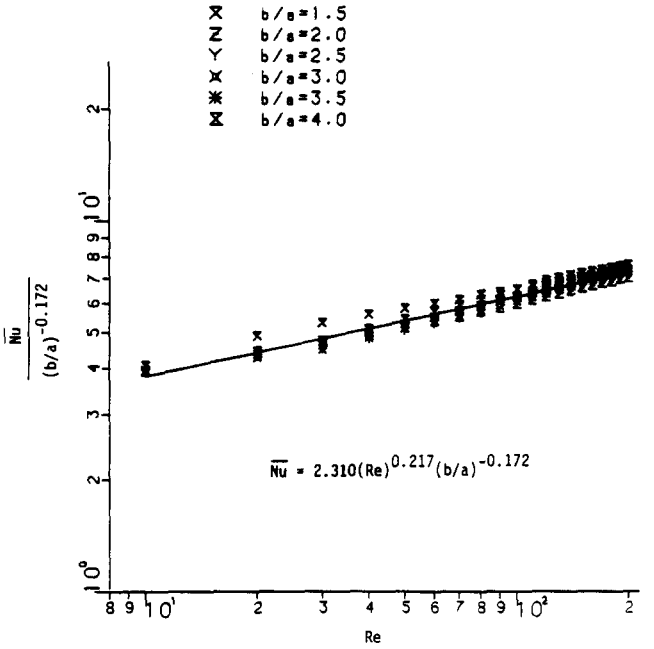

Figure 15 Correlation of Nusselt number for the third droplet of nonvaporizing three-droplet array

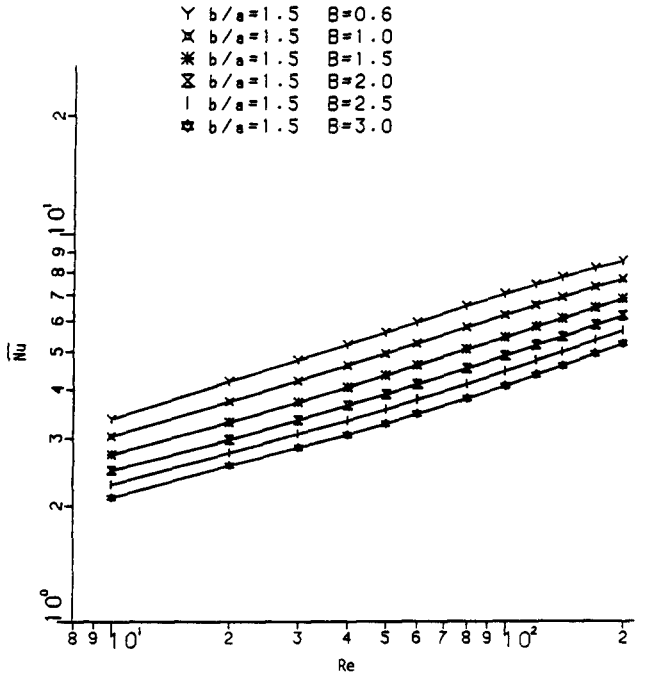

Figure 16 Average Nusselt number for the first droplet of vaporizing three-droplet array

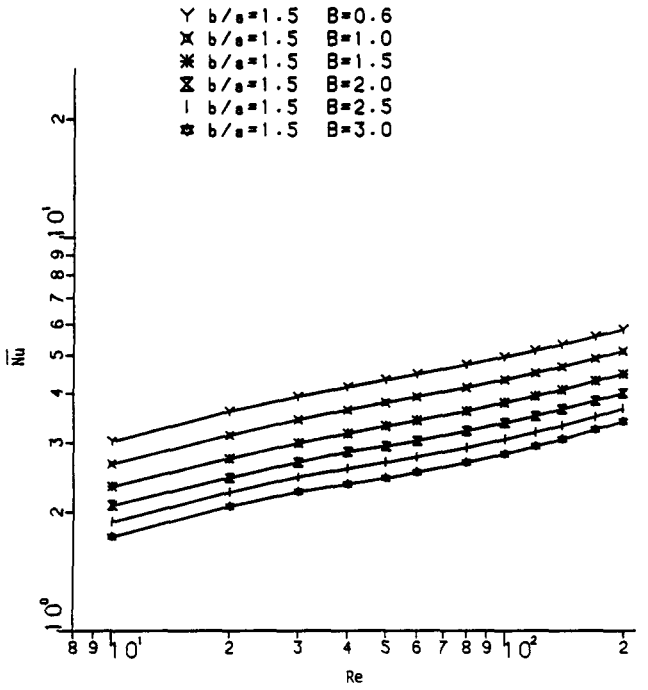

Figure 17 Average Nusselt number for the second droplet of vaporizing three-droplet array

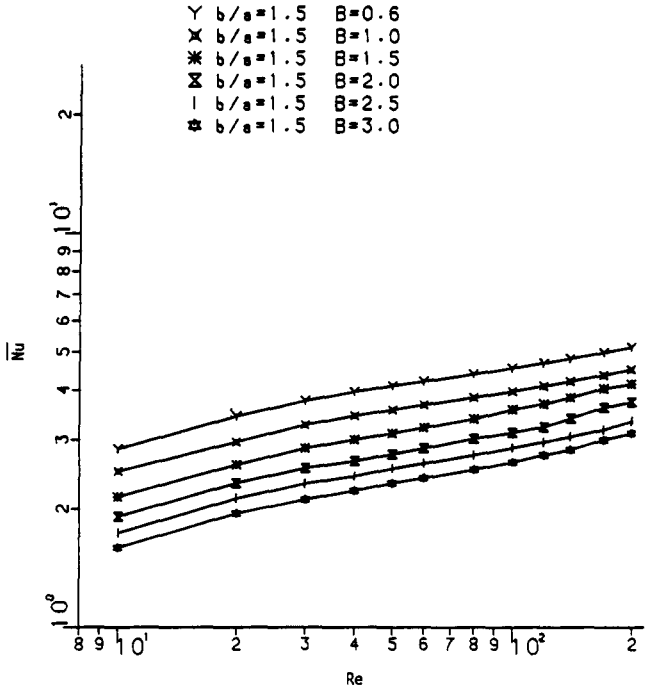

Figure 18 Average Nusselt number for the third droplet of vaporizing three-droplet array

applied directly as an input for a complete liquid spray analysis. The correlation obtained for the second droplet would be the most appropriate one.

The one drawback in the present nonuniform mesh geometry is that it does not have a uniformly fine grid along the droplet surface. Therefore the accuracy of the solution will be affected by relatively coarser grids in spite of the fine spacings in some other regions of the droplet surface. A grid generation scheme to improve numerical accuracy is currently underway. The results of that study will be reported in a forthcoming publication.

Conclusion

The effects of droplet spacing on the heat and mass transfer characteristics of an individual droplet in a liquid fuel spray was studied. A cylindrical cell model with nonuniform grid spacing was used. The Navier-Stokes equations expressed in vorticity-

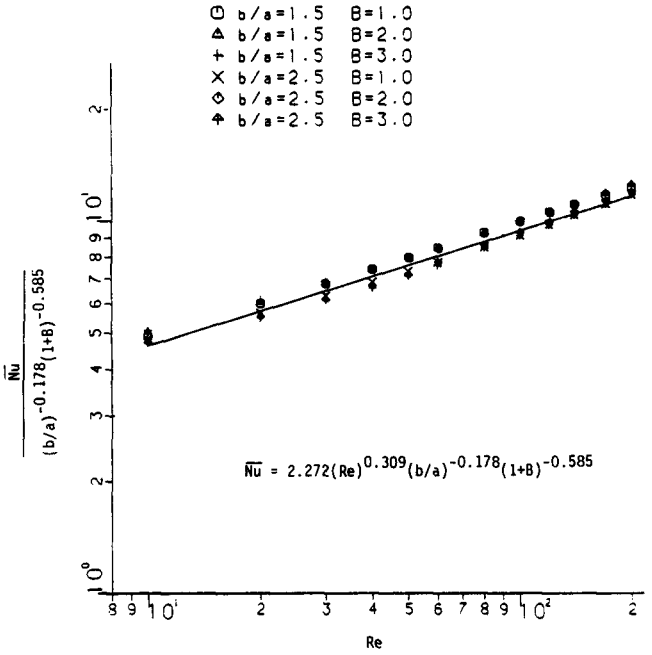

Figure 19 Correlation Nusselt number for the first droplet of vaporizing threee-droplet array

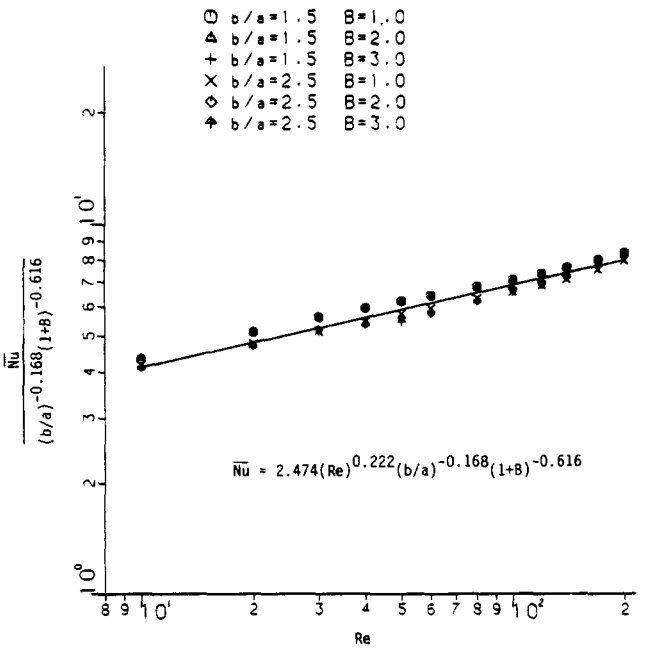

Figure 20 Correlation Nusselt number for the second droplet of vaporizing three-droplet array

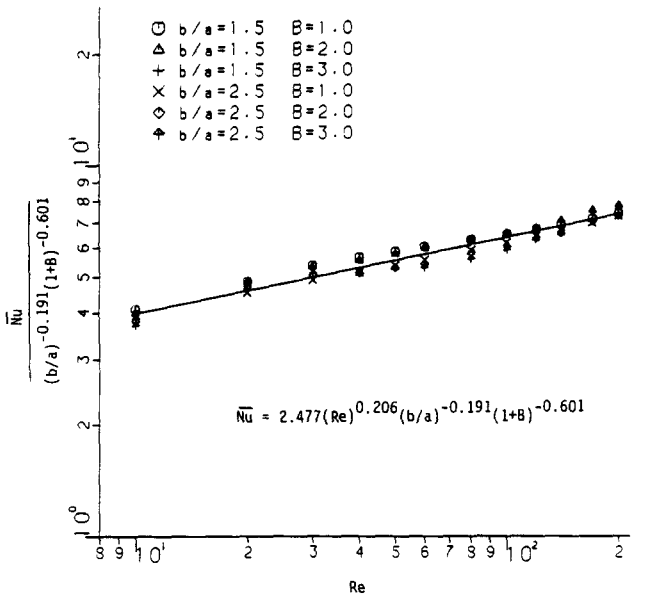

Figure 21 Correlation Nusselt number for the third droplet of vaporizing three-droplet array

stream-function form and the energy equation are solved numerically by a hybrid scheme. Nusselt number correlations of individual droplets for both the vaporizing and the nonvaporizing droplet array have been obtained. These correlations, which include droplet interaction, can be used for a more complete spray model.

Acknowledgment

The authors acknowledge support for this research by the National Science Foundation under research grant MEA-8404292.

References

1 Williams, A. Combustion of droplets of liquid fuels: A review. *Combustion and Flame*, 1973, **21**, 1–31

2 Faeth, G. M. Current status of droplet and liquid combustion. *Prog. Energy Combust. Sci.*, 1977, **3**, 191–224

3 Law, C. K. Recent advances in droplet vaporization. *Prog. Energy Combust. Sci.*, 1982, **8**, 171–201

4 Sirignano, W. A. Fuel droplet vaporization and spray combustion. *Prog. Energy Combust. Sci.*, 1983, **9**, 291–322

5 Tal, R. and Sirignano, W. A. Cylindrical cell model for the hydrodynamics of particle assemblages at intermediate Reynolds numbers. *AICHE J.*, 1982, **28**, 233–237

6 Tal, R., Lee, D. N., and Sirignano, W. A. Hydrodynamics and heat transfer in sphere assemblages—cylindrical cell models. *Int. J. Heat Mass Transfer*, 1983, **26**, 1265–1273. Also see ASME preprint 81-WA/HT-44 (1981) and AIAA preprint 82-0302 (1982)

7 Tal, R., Lee, D. N., and Sirignano, W. A. Heat and momentum transfer around a pair of spheres in viscous flow. *Int. J. Heat Mass Transfer*, 1984, **27**, 1953–1962

8 Tal, R., Lee, D. N., and Sirignano, W. A. Periodic solutions of heat transfer for flow through a periodic assemblage of spheres. *Int. J. Heat Mass Transfer*, 1984, **27**, 1414–1417

9 Prakash, S. Unsteady theory of droplet vaporization with large gas and liquid Reynolds numbers. Ph.D. Thesis, Princeton University, Princeton, N.J., 1978

10 Patankar, S. V. *Numerical Heat Transfer and Fluid Flows*. Hemisphere, 1980

11 Renksizbulut, M. and Yuen, M. C. Numerical study of droplet evaporation in a high-temperature stream. *ASME J. Heat Transfer*, 1983, **105**, 384–388

12 LeClair, B. P., Hamielec, A. E., Pruppacher, H. R., and Hall, W. D. A theoretical and experimental study of the internal circulation in water drops falling at terminal velocity in air. *J. Atmospheric Sci.*, 1972, **29**, 728–740